Efficient second harmonic generation between photonic and plasmonic modes in a tunable transparent conducting oxide waveguide

Fu Xu (许 福)† and Yu Sun (孙 钰)*,†

School of Information Science and Technology, Beijing Forestry University, Beijing 100083, China
**Corresponding author: sunyv@bjfu.edu.cn*

Received October 30, 2015; accepted December 24, 2015; posted online February 22, 2016

Efficient second harmonic generation (SHG) in a nonlinear transparent conducting oxide (TCO) stripe waveguide that incorporates an organic polymer is theoretically investigated. The phase match condition between the fundamental photonic mode at the second harmonic and the fundamental long-range plasmonic mode at the fundamental frequency can be satisfied by dynamically or statically tuning the free carrier concentration of the TCO. The theoretically generated signal reaches its maximum up to 56.4 mW at a propagation distance of 34.8 μm for a pumping power of 1 W. The corresponding normalized conversion efficiency of the phase-matched SHG is up to 4.65×10^3 $W^{-1}\,cm^{-2}$.

OCIS codes: 190.2620, 190.4390.
doi: 10.3788/COL201614.031901.

Among nonlinear processes, second harmonic generation (SHG) is frequently studied for its concise principles, simple implementation, and extensive applications[1–3]. Due to the dramatic locally enhanced confinement of light beyond the diffraction limit, plasmonic-based structures are among the most promising candidates for nonlinear devices[4]. Enhanced SHGs have been presented in a variety of metallic nanostructures, including plasmonic slot waveguides[5], long-range plasmonic waveguides[6], and hybrid plasmonic waveguides[7–9]. Although the aforementioned approaches reveal the potential of efficient frequency doubling, all of these structures incorporate noble metals as plasmonic materials and are electrically passive. In plasmonic waveguides, the phase-matching condition is usually fulfilled via the modal phase-matching technique by statically engineering the geometric parameters, which require the fabrication of an array of nonlinear waveguides with gradual changes. The intrinsic Ohm loss of the metal reduces the distance of interaction between different frequencies and in turn limits the efficiency of the SHG.

Pioneering works in the search for new plasmonic materials have reported that transparent conducting oxides (TCOs) are promising CMOS-compatible, low-loss materials with tunable optical properties[10,11]. The application of the electric field by external gates results a charge depletion or accumulation in TCOs, which tunes its permittivity by shifting the plasma frequency[12,13]. Based on the extraordinary tuning capabilities of TCOs, active components in the linear regime have been intensively studied[12–14]. Conversely, nonlinear optical processes associated with TCOs remain relatively unexplored compared with their linear counterparts.

In this Letter, we propose a nonlinear TCO stripe waveguide that incorporates an organic polymer for an SHG and incorporates a tunable TCO material. As schematically illustrated in Fig. 1, a thin layer of TCO is sandwiched between a doped, cross-linked organic polymer with a nonlinear susceptibility of $\chi^{(2)}_{111} = 619$ pm/V[5,15] and a refractive index of $n = 1.643$[16]. The cladding material is silica. To focus on the tunability of TCO, the width of the waveguide, the thickness of the polymer, and the TCO are fixed at $w = 2.5$ μm, $t_p = 1.5$ μm, and $t_t = 25$ nm, respectively. The TCO selected for SHG in this Letter is Ga-doped zinc oxide (GZO), which is described by the Drude–Lorentz oscillator model as follows[17]:

$$\varepsilon(\omega) = \varepsilon_\infty - \frac{\omega_p^2}{\omega(\omega + i\Gamma_p)} + \frac{f_1\omega_1^2}{(\omega_1^2 - \omega^2 - i\omega\Gamma_1)}, \quad (1)$$

where the experimentally obtained background permittivity $\varepsilon_\infty = 2.475$, the unscreened plasma frequency $\omega_p = 1.927$ eV, and the collision frequency $\gamma = 5.07 \times 10^{16}$ rad/s. The carrier relaxation rate $\Gamma_p = 0.117$ eV. The strength, center frequency, and damping of the Lorentz oscillator

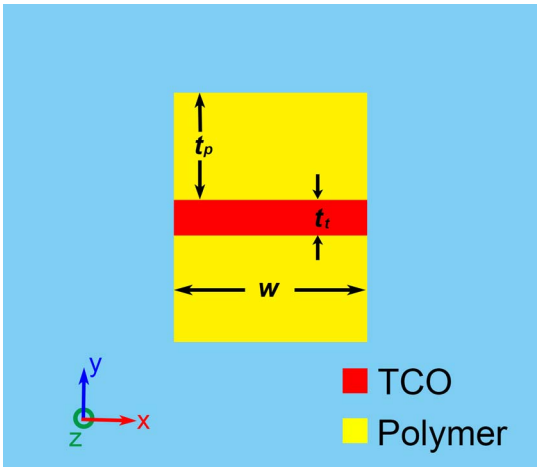

Fig. 1. Schematic of the nonlinear TCO stripe waveguide.

are $f_1 = 0.866$, $\omega_1 = 4.850$ eV, and $\Gamma_1 = 0.029$ eV, respectively[17]. The unscreened plasma frequency ω_p is determined by

$$\omega_p^2 = \frac{Ne^2}{\varepsilon_0 m^*}, \tag{2}$$

where N is the carrier concentration, and the effective optical mass of the conducting electrons is m^*[11]. A carrier concentration of $N_0 = 9.426 \times 10^{20}$ cm^{-3} is used in the m^* fitting[13]. The real part of GZO's permittivity ε' at the fundamental frequency (FF, 1960 nm) and the second harmonic (SH, 980 nm) for carrier concentrations from $0.5N_0$ to $2N_0$[18] is shown in Fig. 2. The value of ε' is positive at the SH with the low carrier concentration, so the TCO is dielectric like and the proposed waveguide supports the photonic mode as the stripe dielectric waveguide. The value of ε' is negative at the FF, so the TCO is metal like and the waveguide supports the long-range plasmonic mode[19].

Except for the statically changing geometric parameters in the metal-based structure, the phase match condition in the proposed TCO strip waveguide can be satisfied by either statically controlling the fabrication conditions[17,18], or by dynamically tuning the external gates as in TCO-based modulators[12,13]. Figure 3 illustrates the effective indices $\mathrm{Re}(n_{\mathrm{eff}})$ of the interacting modes as functions of the carrier concentration. The cross point ($N = 0.57N_0$) in Fig. 3 indicates that the phase match can be satisfied between the fundamental TM photonic mode at the SH and the fundamental TM long-range plasmonic mode at the FF by tuning the applied electric field. Then, the TCO parameter should fixed at the phase- matching point for continuous SHG. At the phase match point, the TCO permittivity is $-1.839 + 0.962i$ at the FF and $2.072 + 0.125i$ at the SH, and the complex effective index N_{eff} of the plasmonic mode at the FF and the photonic mode at the SH are $1.625 + 1.249 \times 10^{-2}i$ and $1.625 + 7.139 \times 10^{-4}i$, respectively. Due to the lower material loss of the TCO at the SH and lower field concentration in a lossy TCO of the photonic mode, the propagation loss of the photonic mode at the SH is almost two orders of magnitude smaller than that of the FF mode. So the SH mode propagates much longer than the pump FF mode after its nonlinear generation.

Figures 4(a) and 4(b) shows the mode profiles of the strip waveguides at the phase match point, as calculated by the commercial finite-element method solver COMSOL™. In order to see the modal profiles more clearly, we plot in Fig. 5 the normalized $|Ey|$ distributions along the y cutline at the center of the waveguide. Both Figs. 4 and 5 indicate a large spatial overlap without

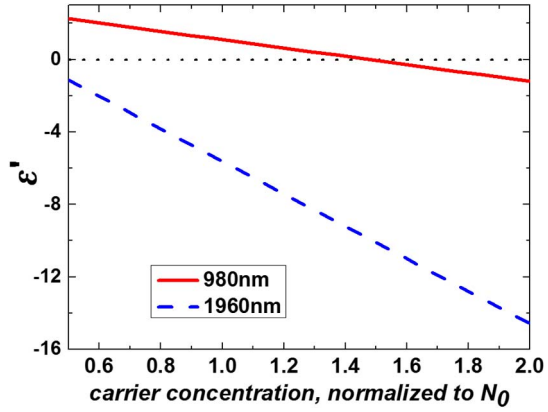

Fig. 2. Real part of GZO's permittivity versus its carrier concentration at the FF (1,960 nm) and the SH (980 nm).

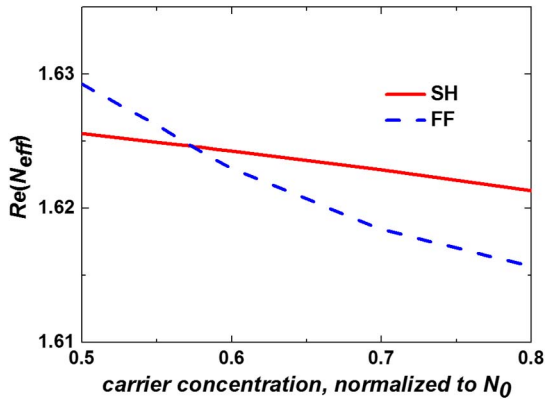

Fig. 3. Phase match condition.

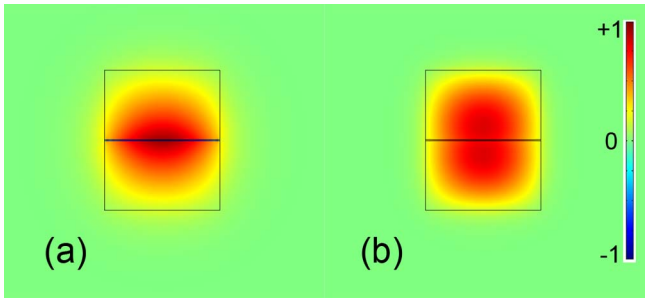

Fig. 4. E_y distributions of the fundamental TM (a) long-range plasmoic mode at the FF and (b) photonic mode at the SH.

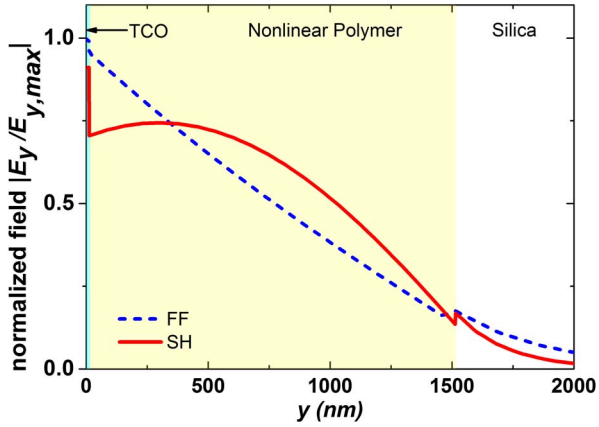

Fig. 5. Normalized field $|E_y/E_{y,\max}|$ distributions on the center line along the y direction.

cancellation in the nonlinear integration area (i.e., the polymeric region). The nonlinear coupling coefficients (NCCs) between the interacting modes in SHG are defined as[5]:

$$\kappa_1 = \varepsilon_0 \iint [\chi^{(2)}{:}E_{\mathrm{SH}}(x,y)E^*_{\mathrm{FF}}(x,y) \cdot E_{\mathrm{FF}}(x,y)]\mathrm{d}x\mathrm{d}y$$
$$\kappa_2 = \varepsilon_0 \iint [\chi^{(2)}{:}E_{\mathrm{FF}}(x,y)E_{\mathrm{FF}}(x,y) \cdot E_{\mathrm{SH}}(x,y)]\mathrm{d}x\mathrm{d}y, \quad (3)$$

where $E(x,y)$ is the normalized modal profile. The NCC values are $\kappa_1 = \kappa_2^* = 1.01 \times 10^2$ ps/m/W$^{1/2}$ at the phase match point. Though there are other modes at the SH near the fundamental surface photonic mode in term of their effective indices, the SHG of these modes is neglectable due to the four-orders- smaller NCC caused by the modal overlap integral cancellation.

Then, the SHG process is investigated by numerically solving the nonlinear coupling wave equations for lossy waveguides, as follows[5,20]:

$$\frac{\partial A_{\mathrm{FF}}}{\partial z} = -\frac{\alpha_{\mathrm{FF}}}{2}A_{\mathrm{FF}} + i\frac{\omega}{4}\kappa_1 A^*_{\mathrm{FF}}A_{\mathrm{SH}}\exp(i\Delta\beta z)$$
$$\frac{\partial A_{\mathrm{SH}}}{\partial z} = -\frac{\alpha_{\mathrm{SH}}}{2}A_{\mathrm{SH}} + i\frac{\omega}{4}\kappa_2^* A_{\mathrm{FF}}A_{\mathrm{FF}}\exp(-i\Delta\beta z), \quad (4)$$

where A is the slowly varying complex modal amplitude, $\Delta\beta = \beta_{\mathrm{SH}} - 2\beta_{\mathrm{FF}}$ is the phase mismatch in SHG, and $\alpha = 4\pi\,\mathrm{Im}(N_{\mathrm{eff}})/\lambda$ is the attenuation coefficient. The wave number is defined as $\beta = 2\pi\mathrm{Re}(N_{\mathrm{eff}})/\lambda$. To evaluate the efficiency of the SHG, a normalized conversion efficiency[21] is defined as the factor of merit (FoM): $\eta = P_{\mathrm{SH}}(L_p)/(P_{\mathrm{FF}}(0)L_p)^2$, where $P_{\mathrm{FF}}(0)$ is the pump power of the FF, L_p is the length when the generated SH reaches its maximum, and $P_{\mathrm{SH}}(L_p)$ is the corresponding maximum output power.

Figure 6 shows the SHG process along a propagation of 150 μm pumped by an FF power of 1 W. The pump power decreases monotonously due to the nonlinear conversion and high propagation loss, while the power of the generated SH signal ramps up quickly due to the efficient energy feed from the FF through nonlinear wavelength conversion and separates from the pump due to the lower propagation loss. Due the phase match between the interacting modes, the SH signal builds up coherently without oscillation over the entire length of waveguide. The SH signal reaches its maximum up to 56.4 mW at a propagation distance of 34.8 μm. The corresponding normalized conversion efficiency is up to 4.65×10^3 W^{-1} cm^{-2}.

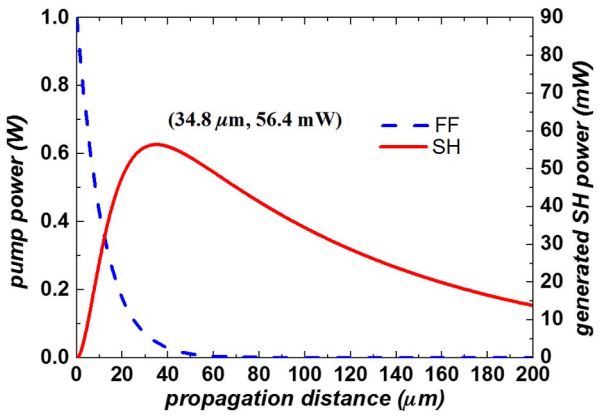

Fig. 6. Intensity variations in the propagation with a pump power of 1 W.

In conclusion, we theoretically propose a nonlinear TCO stripe waveguide for an efficient SHG process. Instead of statically adjusting the geometric parameters, the phase match condition between the fundamental TM photonic mode at the SH and the fundamental TM long-range plasmonic mode at the FF can be satisfied by dynamically or statically tuning the carrier concentration of TCO. The generated SH signal can travel over a relatively long distance after the depletion of the pump due to the low propagation loss of the photonic mode. The capability of supporting efficient SHG makes the tunable TCO stripe waveguide a promising substitution for metal-based plasmonic structures as nonlinear wavelength conversion devices in integrated nanophotonic circuits.

The authors would like to thank Prof. Eric Cassan at the Institut d' Electronique Fondamentale of Université Paris-Sud for his valuable technical advice. This work was supported by the Fundamental Research Funds for the Central Universities under Grant Nos. TD2014-01 and BLX2014-26.

†Both authors contributed equally to this work.

References

1. R. W. Boyd, *Nonlinear Optics* (Academic press, 2003).
2. C. Ma, Y. Wang, L. Liu, X. Fan, A. Qi, Z. Feng, F. Yang, Q. Peng, Z. Xu, and W. Zheng, Chin. Opt. Lett. **12**, 030501 (2014).
3. B. Zhang, J. Ning, Z. Wang, K. Han, and J. He, Chin. Opt. Lett. **13**, 051402 (2015).
4. W. Cai, A. P. Vasudev, and M. L. Brongersma, Science **333**, 1720 (2011).
5. J. Zhang, E. Cassan, D. Gao, and X. Zhang, Opt. Express **21**, 14876 (2013).
6. J. Zhang, P. Zhao, E. Cassan, and X. Zhang, Opt. Lett. **38**, 848 (2013).
7. J. Zhang, E. Cassan, and X. Zhang, Opt. Lett. **38**, 2089 (2013).
8. F. F. Lu, T. Li, X. P. Hu, Q. Q. Cheng, S. N. Zhu, and Y. Y. Zhu, Opt. Lett. **36**, 3371 (2011).
9. H. Yin, Y. Liu, Z. Yu, Q. Shi, H. Gong, X. Wu, and X. Song, Chin. Opt. Lett. **11**, 101901 (2013).
10. G. V. Naik and A. Boltasseva, Metamaterials **5**, 1 (2011).
11. P. R. West, S. Ishii, G. V. Naik, N. K. Emani, V. M. Shalaev, and A. Boltasseva, Laser Photon. Rev. **4**, 795 (2010).
12. Z. Lu, W. Zhao, and K. Shi, IEEE Photonics J. **4**, 735 (2012).
13. V. E. Babicheva, N. Kinsey, G. V. Naik, M. Ferrera, A. V. Lavrinenko, V. M. Shalaev, and A. Boltasseva, Opt. Express **21**, 27326 (2013).
14. A. Krasavin and A. Zayats, Phys. Rev. Lett. **109**, 053901 (2012).
15. Y. Enami, C. Derose, D. Mathine, C. Loychik, C. Greenlee, R. Norwood, T. Kim, J. Luo, Y. Tian, and A.-Y. Jen, Nat. Photonics **1**, 180 (2007).
16. X. Yang, J. Yao, J. Rho, X. Yin, and X. Zhang, Nat. Photonics **6**, 450 (2012).

17. K. Jongbum, G. V. Naik, N. K. Emani, U. Guler, and A. Boltasseva, IEEE J. Sel. Top. Quantum Electron. **19**, 4601907 (2013).
18. D. C. Look, T. C. Droubay, and S. A. Chambers, Appl. Phys. Lett. **101**, 102101 (2012).
19. P. Berini, Adv. Opt. Photonics **1**, 484 (2009).
20. Z. Ruan, G. Veronis, K. L. Vodopyanov, M. M. Fejer, and S. Fan, Opt. Express **17**, 13502 (2009).
21. K. R. Parameswaran, R. K. Route, J. R. Kurz, R. V. Roussev, M. M. Fejer, and M. Fujimura, Opt. Lett. **27**, 179 (2002).